Chiral Order and Electromagnetic Dynamics in One-Dimensional Multiferroic Cuprates

Shunsuke Furukawa,* Masahiro Sato, and Shigeki Onoda†

Condensed Matter Theory Laboratory, RIKEN, Wako, Saitama 351-0198, Japan

(Received 5 July 2010; revised manuscript received 24 October 2010; published 14 December 2010)

We show by unbiased numerical calculations that the ferromagnetic nearest-neighbor exchange interaction stabilizes a vector spin chiral order against the quantum fluctuation in a frustrated spin-$\frac{1}{2}$ chain relevant to multiferroic cuprates, $LiCu_2O_2$ and $LiCuVO_4$. Our realistic semiclassical analyses for $LiCu_2O_2$ resolve controversies on the helical magnetic structure and unveil the pseudo-Nambu-Goldstone modes as the origin of experimentally observed electromagnons.

DOI: 10.1103/PhysRevLett.105.257205 PACS numbers: 75.10.Jm, 75.40.Gb, 75.80.+q, 77.80.−e

Parity symmetry may be broken spontaneously in magnets [1–3] even if the original crystal structure preserves it. It occurs, for instance, when the vector chirality [3] $\boldsymbol{\kappa}_{r,r'} = \langle \boldsymbol{S}_r \times \boldsymbol{S}_{r'} \rangle$ of neighboring spins $\boldsymbol{S}_r$ and $\boldsymbol{S}_{r'}$ acquires a nonzero macroscopic average in geometrically frustrated magnets [Fig. 1(a)]. The helical magnetism [1,2] in which the spins align in a helix with a particular handedness is a typical example. This issue of the spin chiral order [3] and the associated electromagnetic excitations have been highlighted by a recently discovered multiferroic behavior, a ferroelectricity induced by a spin cycloid [4,5]. In spite of theoretical advances in the understanding of the static magnetoelectric effect [6–8], the dynamical effects [9–12] remain controversial.

In helical magnets, three Nambu-Goldstone modes appear in principle [1,2] since the SU(2) symmetry of the spins are fully broken. In the case of the spin cycloid [Fig. 1(b)], one corresponds to a phason describing an infinitesimal change of the pitch of the cycloid [Fig. 1(c)]. The other two represent infinitesimal rotations of the cycloid plane [Fig. 1(d)]. Because of magnetic anisotropy, they usually acquire an energy gap and can then be probed with the antiferromagnetic resonance [13]. These modes may also be excited by the electric component of light through the magnetoelectric coupling. Recent THz spectroscopy experiments on $R\mathrm{MnO}_3$ [9,10] have demonstrated that this electromagnon spectrum grows below the ferroelectric transition temperature. However, because of the large $GdFeO_3$-type distortion, the observed spectrum is dominated by high-energy magnons at the Brillouin-zone boundary [10] through the magnetostriction mechanism [14]. The roles of the Nambu-Goldstone modes remain open [11].

The ferroelectricity associated with the spin cycloid has also been found in quasi-one-dimensional (Q1D) cuprates, $LiCu_2O_2$ [15] and $LiCuVO_4$ [16]. These spin-chain compounds are advantageous in observing the lowest-energy magnons in the optical spectrum since the crystal structure is less distorted along the chains. In particular, in $LiCu_2O_2$, the contribution from the zone-boundary magnons along the chain is prohibited by the symmetry. However, the understanding of experimental findings on the Q1D multiferroic cuprates remains controversial, including the magnetic ordering pattern [12,17–20] and the dynamical properties [12] in $LiCu_2O_2$. Furthermore, it is by far nontrivial from the theoretical viewpoint whether the chiral long-range order (LRO) parasitic to the helical magnetism can be stabilized against quantum fluctuations. In fact, strong quantum fluctuations in one dimension often lead to a valence-bond order accompanied by a moderately large gap in the spin excitations [21,22]. This spin gap can prevail over weak interchain couplings and prevent the helical magnetic LRO, as in $CuGeO_3$ [23]. A possibility that the chiral ordered phase can appear for a weak easy-plane anisotropy in the frustrated spin-$\frac{1}{2}$ chain has

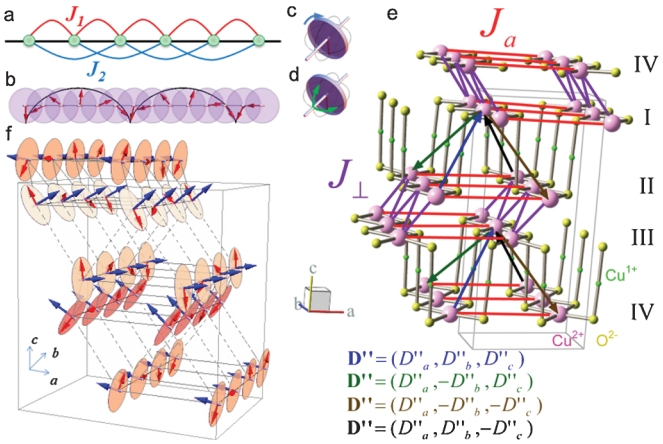

FIG. 1 (color). (a) A 1D frustrated spin model with J_1 and $J_2(>0)$ being the nearest-neighbor and second-neighbor exchange couplings. (b) A spin cycloid in the propagation direction of the $J_1 - J_2$ spin chain. Spins rotate within the common plane represented by the disks. (c),(d) Three Nambu-Goldstone modes in the SU(2)-symmetric model: a phason [(c)] and two rotation modes of the spiral plane [(d)]. (e) Cu^{2+}, Cu^{1+} and O^{2-} ions in $LiCu_2O_2$, and interchain Heisenberg exchange ($J_{a,\perp}$) and interlayer Dzyaloshinskii-Moriya interactions. On the arrows with four different colors, four distinct DM vectors ($\boldsymbol{D}''$) are assigned. (f) Hypothetical magnetic structure (red arrows) and lowest-energy spin-excitation mode (rotations around blue arrows) in the THz range for $LiCu_2O_2$.

been addressed [24,25], and conclusive calculations are called for.

In this Letter, we develop a comprehensive theory for Q1D multiferroic cuprates. We uncover that the ferromagnetic nearest-neighbor exchange coupling J_1 stabilizes a chiral order in the frustrated spin-$\frac{1}{2}$ chain under weak easy-plane anisotropy, in sharp contrast to the case of the antiferromagnetic J_1 [Fig. 2(b)]. With weak three-dimensional (3D) couplings, this roughly controls whether the ground state exhibits the helical magnetic order or the Néel or dimer order. Our phase diagram is useful for classifying several Q1D cuprates [26,27] [Fig. 2]. We also theoretically clarify the magnetic ordering structure and the electromagnetic excitation spectra in $LiCu_2O_2$, which show overall agreements with experiments [12,15,17–20]. These agreements give evidence that weak interchain couplings and magnetic anisotropy allow the electric component of light to excite otherwise zero-energy Nambu-Goldstone modes.

We first reveal the origin of the vector chiral order underlying the spin spiral in $LiCuVO_4$ and $LiCu_2O_2$. At higher temperatures than the interchain couplings of order of the Néel temperature (2.5 K and 24 K for $LiCuVO_4$ and $LiCu_2O_2$, respectively), they are described in terms of a one-dimensional (1D) spin-$\frac{1}{2}$ model [Fig. 1(a)],

$$H_{1D} = \sum_{n=1,2} J_n \sum_j (S_j^x S_{j+n}^x + S_j^y S_{j+n}^y + \Delta S_j^z S_{j+n}^z), \quad (1)$$

($J_2 > 0$) with the electronic spin $\boldsymbol{S}_j = (S_j^x, S_j^y, S_j^z)$ at the Cu^{2+} site j in the chain, and the small symmetric easy-plane exchange anisotropy $0 < 1 - \Delta \ll 1$. In the classical limit, a helical magnetic ground state is realized for $|J_1|/J_2 < 4$ [Fig. 2(a)], with a finite uniform vector spin chirality $\langle \kappa_{j,j+1}^z \rangle = \kappa^z$. In the quantum spin-$\frac{1}{2}$ case, this chiral order tends to yield to valence-bond orders [21,22]. However, our previous finite-size calculation of the spin Drude weight, supplemented by the bosonization analysis, has suggested that the chiral phase might survive in a wider range for ferromagnetic J_1 [25]. To precisely determine the ground-state phase diagram in a conclusive manner, we have performed numerical calculations based on the time evolving block decimation algorithm for an infinite system (iTEBD) [28,29]. Figure 2(b) presents the global phase diagram and a profile of the chiral order parameter κ^z in the space of J_1/J_2 and Δ. It confirms that the chiral phase extends over a wide region for ferromagnetic $J_1 < 0$. In particular, the chiral order is pronounced by small magnetic anisotropy $1 - \Delta > 0$ and a moderate value of $|J_1|/J_2$ that roughly correspond to the multiferroic cuprates. This chiral LRO is stable up to a close vicinity of the SU(2)-symmetric case $\Delta = 1$, where it is replaced with a dimer order. It is also replaced with another dimer order having a unit of $|\uparrow\downarrow\rangle + |\downarrow\uparrow\rangle$ by stronger anisotropy $0 \leq \Delta \lesssim 0.6$. On the other hand, for antiferromagnetic $J_1 > 0$, the singlet-dimer order accompanied by the spin gap is robust [21,22].

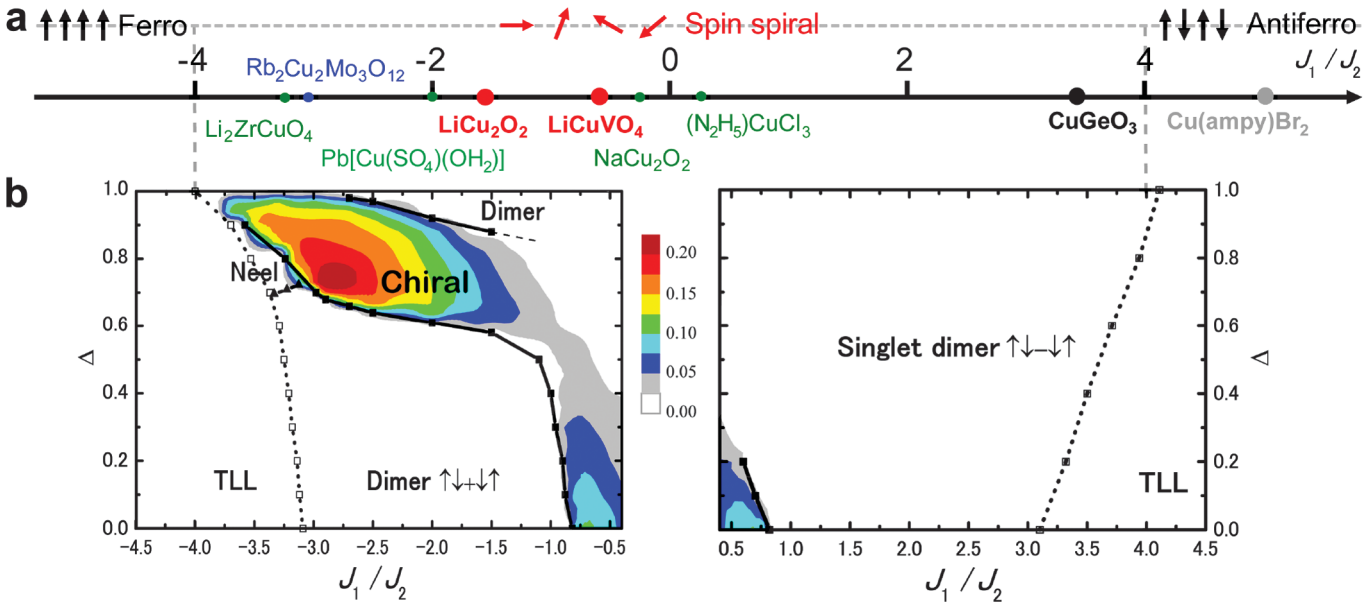

FIG. 2 (color). Ground-state phase diagram of the spin-chain model H_{1D}. (a) The classical phase diagram and relevant Q1D spin-$\frac{1}{2}$ materials. Estimates of J_1/J_2 for materials are taken from Refs. [17,26,27]. The materials shown in green exhibit an antiferromagnetic LRO, but their detailed magnetic structures have not been established yet. In $Rb_2Cu_2Mo_3O_{12}$, a magnetic LRO has not been detected down to 2 K [26]. Usually, $1 - \Delta \lesssim 0.05$ in cuprates. (b) The quantum phase diagram and the map of the chiral order parameter κ^z for $S = \frac{1}{2}$. The horizontal axis J_1/J_2 is the same as in the panel (a). The boundary between the dimer phase and the chiral phase in the case of $J_1 > 0$ agrees with the previous numerical study [22]. For $|J_1|/J_2 \gtrsim 4$, Tomonaga-Luttinger liquid (TLL) phases appear. Detailed methods of identifying each phase and the phase boundaries are explained in the supplementary material [29]. It was difficult to determine the phase boundary for small $|J_1|/J_2$ (dashed line).

The above results clearly explain why the Q1D helical magnets or the candidate materials are found dominantly on the ferromagnetic side of J_1 while the materials located on the antiferromagnetic side of J_1 usually show a spin-singlet dimer order or a collinear antiferromagnetic LRO. In real materials having weak interchain couplings, the helical spin quasi-LRO in the chiral phase [24] readily evolves into a genuine helical LRO. Even when the magnetic anisotropy is so small that a material with $J_1 < 0$ is located in a narrow dimer phase near $\Delta = 1$, the spin gap is orders of magnitude smaller than for $J_1 > 0$. Therefore, the weak 3D couplings may close the spin gap and recover the helical magnetic LRO. Once the helical magnetic LRO readily occurs at a finite temperature on the ferromagnetic side of J_1, as in the case of $LiCu_2O_2$, then the static and dynamical properties can be calculated through semiclassical analyses [2]. In the rest of this Letter, constructing a realistic spin model, we will give a theoretical explanation of overall experimental findings on $LiCu_2O_2$.

The material contains four $J_1 - J_2$ spin chains [Fig. 1(a)], each of which lies in one of four stacked ab layers (I to IV) in the unit cell [Fig. 1(e)]. Neutron-scattering experiments [17] have unveiled a magnetic Bragg peak at an incommensurate wave vector $(0.5, 0.173, 0)$ in the reciprocal lattice unit, and the Q1D spin-wave dispersion along the b axis. The observation of the ferroelectric polarization $\boldsymbol{P} \parallel c$ [15,19] and the polarized neutron-scattering experiment [19] indicate the emergence of the uniform bc spin-spiral component in the lowest-temperature phase. Then, a minimal spin model should include the interactions shown in Fig. 1(e). In each layer, the adjacent spin chains along the a axis are coupled via the Heisenberg exchange interaction with moderate coupling strength J_a [Fig. 1(e)]. Two pairs of the adjacent layers, II and III, and IV and I, are also coupled via the nearest-neighbor interchain Heisenberg exchange coupling $J_\perp$ in a zigzag manner [Fig. 1(e)]. On the other hand, a small Heisenberg exchange coupling J' (not shown) between the other two pairs of layers, I and II, and III and IV, induces an incommensurability along the a axis, i.e., $Q_a \neq \pi/a$, which disagrees with the experiment [17,19,20]. To stabilize the experimentally reported uniform bc spiral component [12,15,19,20] and to pin the commensurability along the a axis, the a component of the Dzyaloshinskii-Moriya (DM) vectors for the interlayer DM interactions between I and II and between III and IV is indispensable. This can be provided through the second-neighbor bonds characterized by the four DM vectors $\boldsymbol{D}''$, which are specified by the amplitudes of the a, b, and c components D''_a, D''_b, and D''_c [Fig. 1(e)] from the symmetry argument. For simplicity, we take $J' = D''_b = D''_c = 0$. The intrachain DM vectors specified by the amplitude D and the angle θ are uniform within each layer, but the symmetries of the crystal require that their directions alternate in the layer index: $\boldsymbol{D}_{\rm I} = D(\cos\theta, 0, \sin\theta)$, $\boldsymbol{D}_{\rm II} = D(-\cos\theta, 0, \sin\theta)$, $\boldsymbol{D}_{\rm III} = D(\cos\theta, 0, -\sin\theta)$, and $\boldsymbol{D}_{\rm IV} = D(-\cos\theta, 0, -\sin\theta)$. The classical analysis of this model Hamiltonian shows that the intrachain DM interaction rotates the cycloid planes about the b axis from the bc plane by different angles φ_1, φ_2, $-\varphi_1$, and $-\varphi_2$ for the layers I, II, III, and IV, respectively. With the Bragg-peak position $(0.5, 0.173, 0)$ [17], a choice of $(\varphi_1, \varphi_2)/(2\pi) = (-0.08, -0.02)$ reproduce the ^{7}Li nuclear magnetic resonance spectra [18,20] (supplementary Figure S4 [29]). Then, the exchange and DM coupling parameters are determined to reproduce the ordering wave vector $\boldsymbol{Q}$, the rotation angles (φ_1, φ_2) of the spiral planes, the anisotropy in the antiferromagnetic resonance spectra [12]: $(J_1, J_2, J_a, J_\perp, D, D''_a) = (-11.3, 5.9, 1.1, 0.08, 0.37, 0.26)$ meV and $\theta/(2\pi) = 0.43$. It is noteworthy that our choice $(J_1, J_2, J_a, J_\perp)$ is within a reasonable range with respect to previous analyses of inelastic neutron-scattering experiments [17]. The obtained magnetic structure is presented in Fig. 1(f).

The associated Q1D spin-wave dispersions are shown in Fig. 3(a). Magnetic anisotropy has produced the energy gap in otherwise zero-energy Nambu-Goldstone modes at $\boldsymbol{q} = \pm\boldsymbol{Q}$. Since four spins exist in the unit cell, there appear an acoustic branch and three optical branches. The splitting of the four branches is pronounced at the dispersion minima, $\boldsymbol{q} = 0$ and $\boldsymbol{q} = \pm\boldsymbol{Q}$, where we further take account of the bilinear mixing of $\boldsymbol{q} = 0$ and $\boldsymbol{q} = \pm\boldsymbol{Q}$ magnons through the degenerate perturbation theory of interlayer and DM couplings. Figure 3(b) shows the anisotropy of the obtained antiferromagnetic resonance spectra $\mathrm{Im}[\chi^{cc}(\omega) - \{\chi^{aa}(\omega) + \chi^{bb}(\omega)\}/2]$, which remarkably agrees with the experimental result [12]. The lowest-energy mode at $\omega \sim 0.8$ meV is associated with a linear combination of the intralayer phason modes where the change of the pitch of the cycloid in the layers I and II is opposite to that in the layers III and IV [Fig. 1(f)]. It is also accompanied by a small fraction of $2\boldsymbol{Q}$ oscillation. The acoustic mode was observed at $\sim$30 GHz ~ 1 cm$^{-1} \sim 0.12$ meV with the electron spin resonance experiment [13], which is much smaller than the THz frequency of our interest.

Our analyses of magnetoelectric couplings (based on Ref. [14]) show that the dominant contribution to the dielectric absorption spectra arises from the vector chirality on the bonds connecting the adjacent layers (supplementary material [29]). The dominance of the chirality contribution over the magnetostriction sharply contrasts with the case of $R\mathrm{MnO_3}$ [10], and is ascribed to the fact that the unit cell contains only a single spin in the direction of the ordering wave vector. Through this magnetoelectric coupling, most of the spin-wave modes are electric-dipole active. Since main peaks observed in the THz spectroscopy [12] are much sharper than the magnon bandwidth of order of $|J_1|$ and J_2, we take account only of the one-magnon contributions. The anisotropy of thus determined dielectric functions, $\mathrm{Im}[\varepsilon^{cc}(\omega) - \{\varepsilon^{aa}(\omega) + \varepsilon^{bb}(\omega)\}/2]$, shows a reasonable agreement with the experiment [12] [Fig. 3(c)]. As expected, the lowest-energy mode described in Fig. 1(f) has significant amplitude as well. We stress that excitations induced by electric and magnetic components of light appear with comparable amplitude in this system. This is

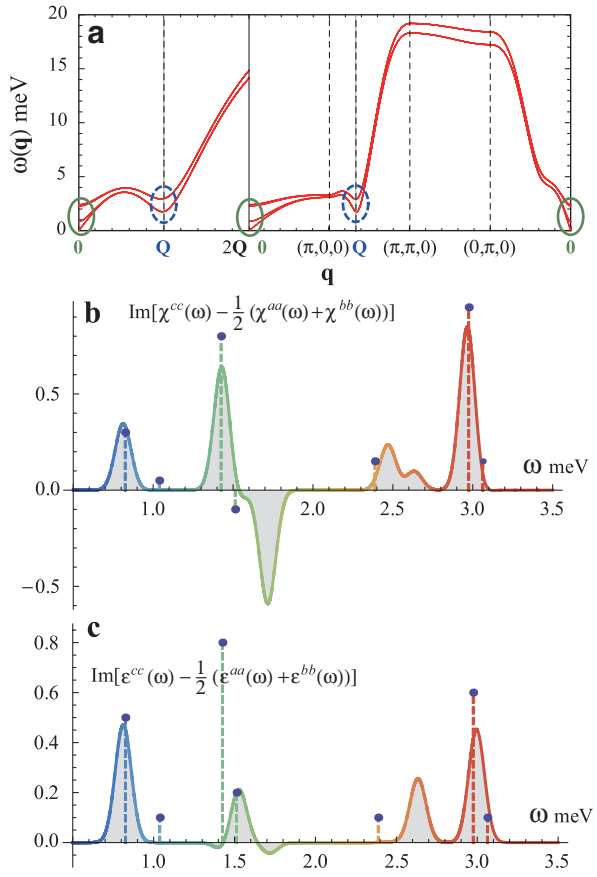

FIG. 3 (color online). Semiclassical analyses for $LiCu_2O_2$. (a) Spin-wave dispersions without taking account of the bilinear coupling among $\boldsymbol{q} = 0, \pm\boldsymbol{Q}$ modes. This coupling only modifies the modes around $\boldsymbol{q} = 0$ and $\pm\boldsymbol{Q}$, marked with solid green and dashed blue circles. The dispersion along the c axis is quite small, since $J_\perp$, $D_a'' < J_a \ll |J_1|$, J_2. (b),(c) Anisotropy in the electromagnetic absorption spectra due to the magnetic and electric components of light, in units of $(g\mu_B)^2$ meV^{-1} and cm^{-1}, respectively. The spectrum consists of 11 gapped modes after the reconstruction of the $\boldsymbol{q} = 0$, $\pm\boldsymbol{Q}$ modes due to their bilinear coupling: $\omega = 0.812$, 1.431, 1.525, 1.717 (doubly degenerate), 2.469, 2.634, 2.977, 2.983, 2.991 (doubly degenerate) meV. Inclusion of even higher harmonics such as $\boldsymbol{q} = \pm 2\boldsymbol{Q}$ modes increases the number of the modes and eventually broadens the peaks. The series of δ-function peaks are replaced with the sum of Gaussians broadened with the width 0.05 meV. Points with dashed lines denote the integrated intensity experimentally observed in the THz spectroscopy [12] in the unit of cm^{-1}. We note that the tilting of the spiral planes crucially changes the signals of electromagnons.

unique to spin-$\frac{1}{2}$ systems free from the magnetostriction contribution to the optics. Then, the magnetoelectric coupling is controlled by quite a small ratio of the relativistic spin-orbit coupling to the on-site Coulomb repulsion.

Dynamical magnetoelectric effects due to the Nambu-Goldstone modes have been identified in the dielectric spectrum of the Q1D spin-$\frac{1}{2}$ multiferroic cuprate $LiCu_2O_2$. Further experiments on Q1D cuprates with weaker 3D couplings as in $LiCuVO_4$ [16,30] and $Rb_2Cu_2Mo_3O_{12}$ [26] might also uncover gapless dielectric spectra due to phasons and chirality solitons [25].

The authors thank T. Rõõm, H. Hüvonen, S.-W. Cheong, T. Arima, Y. Tokura, Y. Yasui, A. Kobayashi, K. Okunishi, and A. Furusaki for discussions. The work was partly supported by Grants-in-Aid for Scientific Research (No. 19052006, No. 20029006, and No. 20046016) from MEXT of Japan and No. 21740275 from JSPS.

*Present address: Department of Physics, University of Toronto, Toronto, Ontario M5S 1A7, Canada.
†s.onoda@riken.jp

[1] A. Yoshimori, J. Phys. Soc. Jpn. **14**, 807 (1959).
[2] T. Nagamiya, *Solid State Physics* (Springer, Berlin, 1967), Vol. 20, pp. 305–411.
[3] J. Villain, Ann. Isr. Phys. Soc. **2**, 565 (1978).
[4] T. Kimura *et al.*, Nature (London) **426**, 55 (2003).
[5] S.-W. Cheong and M. Mostovoy, Nature Mater. **6**, 13 (2007).
[6] H. Katsura, N. Nagaosa, and A. V. Balatsky, Phys. Rev. Lett. **95**, 057205 (2005).
[7] I. A. Sergienko and E. Dagotto, Phys. Rev. B **73**, 094434 (2006).
[8] A. Malashevich and D. Vanderbilt, Phys. Rev. Lett. **101**, 037210 (2008).
[9] A. Pimenov *et al.*, Nature Phys. **2**, 97 (2006).
[10] R. Valdés Aguilar *et al.*, Phys. Rev. Lett. **102**, 047203 (2009).
[11] H. Katsura, A. V. Balatsky, and N. Nagaosa, Phys. Rev. Lett. **98**, 027203 (2007).
[12] D. Hüvonen *et al.*, Phys. Rev. B **80**, 100402(R) (2009).
[13] A. M. Vorotynov *et al.*, Zh. Eksp. Teor. Fiz. **113**, 1866 (1998) [JETP **86**, 1020 (1998)].
[14] C. Jia *et al.*, Phys. Rev. B **76**, 144424 (2007).
[15] S. Park *et al.*, Phys. Rev. Lett. **98**, 057601 (2007).
[16] Y. Naito *et al.*, J. Phys. Soc. Jpn. **76**, 023708 (2007).
[17] T. Masuda *et al.*, Phys. Rev. B **72**, 014405 (2005).
[18] A. A. Gippius *et al.*, Phys. Rev. B **70**, 020406(R) (2004).
[19] S. Seki *et al.*, Phys. Rev. Lett. **100**, 127201 (2008).
[20] Y. Kobayashi *et al.*, J. Phys. Soc. Jpn. **78**, 084721 (2009).
[21] S. R. White and I. Affleck, Phys. Rev. B **54**, 9862 (1996).
[22] T. Hikihara, M. Kaburagi, and H. Kawamura, Phys. Rev. B **63**, 174430 (2001).
[23] M. Hase, I. Terasaki, and K. Uchinokura, Phys. Rev. Lett. **70**, 3651 (1993).
[24] A. A. Nersesyan, A. O. Gogolin, and F. H. L. Eßler, Phys. Rev. Lett. **81**, 910 (1998).
[25] S. Furukawa, M. Sato, Y. Saiga, and S. Onoda, J. Phys. Soc. Jpn. **77**, 123712 (2008).
[26] M. Hase *et al.*, Phys. Rev. B **70**, 104426 (2004).
[27] S.-L. Drechsler *et al.*, Phys. Rev. Lett. **98**, 077202 (2007).
[28] G. Vidal, Phys. Rev. Lett. **98**, 070201 (2007).
[29] See supplementary material at http://link.aps.org/supplemental/10.1103/PhysRevLett.105.257205.
[30] M. Enderle *et al.*, Phys. Rev. Lett. **104**, 237207 (2010).